Noble and alkali adatoms on a $\mathrm{Si(111)}\sqrt{3}\times\sqrt{3}$–Ag surface: a first-principles study

2010 J. Phys.: Condens. Matter 22 085001

(http://iopscience.iop.org/0953-8984/22/8/085001)

J. Phys.: Condens. Matter **22** (2010) 085001 (8pp) doi:10.1088/0953-8984/22/8/085001

Noble and alkali adatoms on a Si(111)$\sqrt{3} \times \sqrt{3}$–Ag surface: a first-principles study

Xin Xie[1], J M Li[1,2,3], W G Chen[1], F Wang[1], S F Li[1], Q Sun[1] and Yu Jia[1,3]

[1] School of Physics and Engineering, Zhengzhou University, Zhengzhou 450052, People's Republic of China
[2] Department of Physics, Henan Institute of Education, Zhengzhou 450053, People's Republic of China

E-mail: jmli@zzu.edu.cn and jiayu@zzu.edu.cn

Received 3 October 2009, in final form 22 December 2009
Published 29 January 2010
Online at stacks.iop.org/JPhysCM/22/085001

Abstract

Using first-principles calculations, we present a comprehensive study on the atomic and electronic structures of metal adatoms (noble metals Ag, Au, Cu and alkali metals Li, Na, K) adsorbed on a Si(111)$\sqrt{3} \times \sqrt{3}$–Ag (hereafter $\sqrt{3}$-Ag) surface. We found that adsorption of noble and alkali adatoms can induce significant structural changes in the topmost Ag layer. The most striking and interesting results are the immersion of the noble and Li adatoms into the substrate Ag layer and the finding of the most stable configurations with three adatoms incorporating into or being adsorbed on the surface dependent on their atomic radii. We also found that the almost empty two-dimensional free-electron-like band s_1 and its band folding s_1^* of the original surface band s_1 of the $\sqrt{3}$-Ag surface split into a gap at the surface Brillouin zone (SBZ) boundary with adsorption of an adatom. The two surface bands gradually move downwards and the s_1 band is gradually filled with an increase of coverage. The s_1 band is fully occupied with the largest band gap ~0.25 eV between the s_1 and s_1^* bands at the critical coverage of 0.14 monolayers (ML) [three adatoms in a Si(111)$\sqrt{21} \times \sqrt{21}$–Ag (hereafter $\sqrt{21}$-Ag) unit cell], which corresponds to the most stable adsorption phase. Although the adsorption configurations are different, both the noble and alkali adatom adsorptions give rise to similar electronic structures at low coverages, indicating a free-electron-like character of the adsorption surfaces.

(Some figures in this article are in colour only in the electronic version)

1. Introduction

Surface superstructures formed by the adsorption of noble metals (Ag, Au, Cu) and alkali metals (Li, Na, K) onto semiconductors have been intensively studied in the past few decades as prototype systems of metal/semiconductor interfaces due to the simple electronic structures of the adatoms [1–4]. However, the adsorption systems may have complex electronic and atomic structures and contain rich physics. The $\sqrt{3}$-Ag surface superstructure is formed by annealing a Si(111)7 × 7 surface covered by one monolayer (ML) of Ag atoms. This adsorption system is one of the most intensively studied surfaces and its atomic structure and electronic properties are now well understood [5–9]. The surface has a nearly ideal two-dimensional free-electron-like surface state and it is believed that the adsorption of noble metals or alkali metals with one loosely bound s electron on the $\sqrt{3}$-Ag surface may lead electron filling into the surface state resulting in high surface electrical conductivity [4, 9, 10].

Experiments found that 0.1–0.2 ML of noble or alkali adatoms deposited on the $\sqrt{3}$-Ag surface could form stable $\sqrt{21}$-Ag(±R10.89°)+ adatom superstructures, which

[3] Authors to whom any correspondence should be addressed.

are regarded as a model for binary surface alloys on semiconductors [4, 11–15]. These surface superstructures produce surface state bands dispersing across the Fermi level (E_F) and exhibit high surface conductivity, and they nowadays play an important role in the investigation of surface state electrical conduction [4, 9, 16, 17]. Based on many different techniques, such as reflection-high-energy electron diffraction (RHEED) [18], scanning tunneling microscopy (STM) [18, 19], angle-resolved ultraviolet photoemission spectroscopy (ARUPS) [11, 13–15], core-level photoemission spectroscopy (CL-PES) [20], and grazing-incidence x-ray diffraction (GIXRD) [12], several atomic structure models have been proposed to elucidate these noble-metal induced $\sqrt{21}$-Ag superstructures. A recent theoretical model proposed by Hojin Jeong *et al* [21] for the noble-metal adatoms on $\sqrt{3}$-Ag suggested that the three-adatom immersed structure on the surface is the most stable phase.

In contrast to the many works on noble-metal adsorption, only a few studies have so far been reported for alkali metals on $\sqrt{21}$-Ag superstructures. Experimentally, alkali metal superstructures have been explored by STM [22, 23], angle-resolved photoemission spectroscopy [4, 9, 11, 13–15], core-level spectroscopy [13, 24] and macro-four-point probe techniques [4, 25], but these works have given us no consensus on the atomic structures of the systems. From a theoretical aspect, Hojin Jeong *et al* [26] studied adsorption of the alkali adatoms Li, Na and K on a $4\sqrt{3} \times 4\sqrt{3}$-Ag surface. However, only the low coverage case was considered in their calculations. To our knowledge, there is no theoretical study of the alkali metals on a $\sqrt{3}$-Ag surface. Thus, theoretical investigation on these systems should be very important in revealing both their atomic and electronic properties.

In this paper, we use a first-principles calculation method to perform a comprehensive study of the adsorption of both noble and alkali metals on the $\sqrt{3}$-Ag surface at different coverages in order to acquire a general picture of the atomic structure and electronic properties of the monovalent-atom-induced $\sqrt{21}$-Ag superstructures and make a comparison between noble and alkali metal adsorption on the surface.

2. Calculation method

In the present research, we carry out first-principles total energy calculations using the Vienna *ab initio* simulation package (VASP) [27] with ultrasoft pseudopotentials [28] and the generalized gradient approximation of Perdew and Wang [29] for the exchange–correlation energy. The surfaces are constructed by repeated slabs with a $\sqrt{3} \times \sqrt{3}$ and a $\sqrt{21} \times \sqrt{21}$ periodicity in surface unit cells. The slabs contain a Ag layer and seven (for $\sqrt{3} \times \sqrt{3}$) or five (for $\sqrt{21} \times \sqrt{21}$) Si layers where a H layer terminates the bottom-most Si layer. A vacuum space of ∼14 Å along the direction normal to the surface is taken, which is large enough to eliminate the interaction of the neighboring slabs. We perform 'accurate' calculations to avoid wrap-around errors [27] and the kinetic energy cutoff is taken at 200 eV to expand wavefunctions within the plane-wave basis. The surface Brillouin zone (SBZ) samplings are employed with 5 × 5 and 2 × 2 k-point meshes for $\sqrt{3} \times \sqrt{3}$ and $\sqrt{21} \times \sqrt{21}$ supercells, respectively. The conjugate gradient scheme is used to obtain the electronic ground state for each atomic configuration, and the Hellmann–Feynman forces are calculated and used to relax the atomic structures. For geometric optimization, all atoms except for the bottom-most Si and H atoms have been relaxed until the force acting on each atom is less than 0.02 eV Å^{-1}. The Si–H distances are fixed at 1.49 Å and the bonds are along the ideal crystalline directions of Si. The calculated lattice constant of the bulk Si (5.46 Å) is used in our calculations.

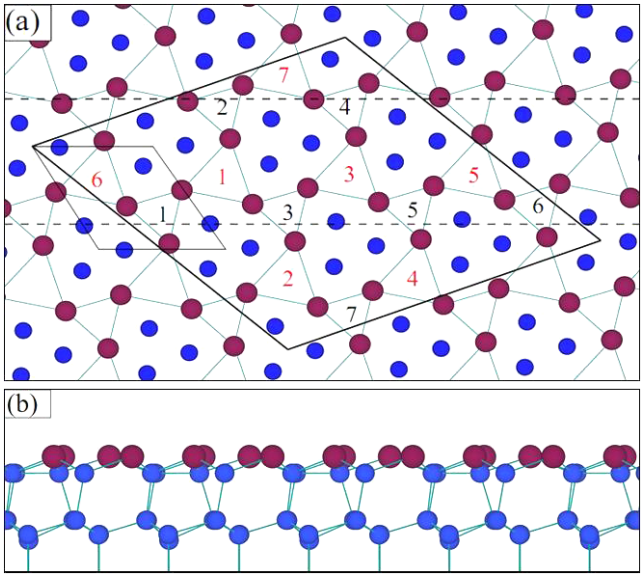

Figure 1. Schematics for (a) top and (b) side views of the atomic structure of the $\sqrt{21}$-Ag surface. The small and large rhombuses drawn by solid lines represent $\sqrt{3}$-Ag and $\sqrt{21}$-Ag unit cells, respectively. The SiT, LT and ST stand for the Si trimer, large Ag triangle and small Ag triangle adsorption sites, respectively. In (b), only the atoms lying between two dashed lines drawn in (a) are shown. The purple and blue spheres represent Ag and Si atoms, respectively. The red and black numbers in the $\sqrt{21}$-Ag unit cell stand for the most stable adsorption sites for the numbers of Na adatoms increasing from one to seven at the ST and LT sites.

3. Results and discussion

3.1. Atomic structures

The atomic structure of the $\sqrt{3}$-Ag surface with the inequivalent triangle (IET) reconstruction has been confirmed by both theory [30, 31] and experiment [31, 32]. This structure contains a small Ag triangle (ST), a large Ag triangle (LT) and a Si trimer (SiT) (see figure 1). Calculated side lengths of the LT and ST are 3.85 and 3.06 Å, which are well consistent with the previous calculation by Jeong (3.88 and 3.00 Å) [26]. For the $\sqrt{3}$-Ag surface there are three adsorption sites, i.e. the centers of the SiT, ST and LT shown in figure 1. In our calculations, the average adsorption energy is defined as

$$E_a = [E_{surf} + NE_{metal} - E_{(surf+Nmetal)}]/N,$$

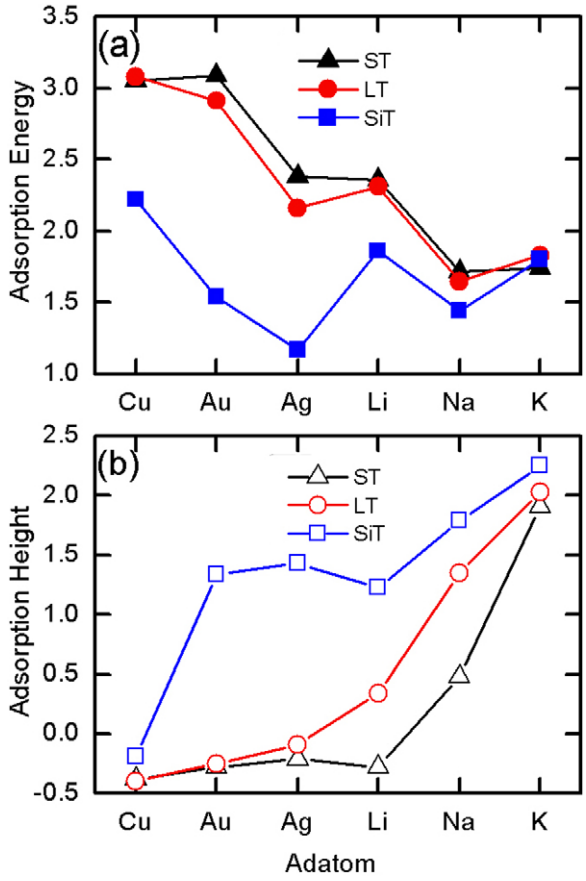

Figure 2. Calculated (a) adsorption energies (eV) and (b) adsorption heights (Å) for noble and alkali metal adatoms adsorbed at the ST, LT and SiT adsorption sites.

where $E_{(\mathrm{surf}+N\mathrm{metal})}$, E_{surf} and E_{metal} are the total energies of the adsorbed system, substrate and isolated metal adatoms, respectively, and N is the number of adatoms adsorbed on the surface.

Firstly, we consider adsorption of a single Ag, Au, Cu, Li, Na or K adatom on the $\sqrt{3}$-Ag surface using a larger $\sqrt{21} \times \sqrt{21}$ surface unit cell. The case corresponds to a low coverage of ∼0.05 ML (1/21 ML). Our calculated adsorption energies and adsorption heights at the three different adsorption sites are displayed in figure 2, and in table 1 we present the values of adsorption energy, adsorption height, distance between the adatom and the nearest substrate Ag atom and side lengths of the LT, ST and SiT where the adatom adsorbs. We find that Au, Ag, Li and Na prefer to adsorb at the ST site. While Cu and K, which have the smallest and largest atomic radii among the considered noble and alkali adatoms, prefer to adsorb at the LT site, though the differences in their adsorption energies at the ST and LT are small (less than 0.1 eV). We should note that for the noble metals the adsorption energies at the ST or the LT are larger than those at the SiT site by more than 1.5 eV. However, for the alkali metals the differences between the adsorption energies at the LT or ST and at the SiT are less than 0.5 eV. An interesting result is that the Cu adatom can immerse in the substrate layer without any energy barrier when it adsorbs at the SiT site due to its small atomic radius.

Table 1. Calculated adsorption energies (E_a), adsorption heights (H_a), distances between the adatoms and the nearest substrate Ag or Si atoms ($d_{\mathrm{adatom-Ag}}$, $d_{\mathrm{adatom-Si}}$) and the side lengths of ST (d_{ST}) and LT (d_{LT}) and SiT (d_{SiT}) for adsorption of a single noble or alkali metal adatom at sites ST (side length 3.06 Å), LT (site length 3.85 Å) and SiT (side length 2.52 Å).

Sites	R_{M} (Å)	Cu 1.28	Au 1.44	Ag 1.45	Li 1.51	Na 1.83	K 2.26
ST	E_a (eV)	3.05	3.09	2.38	2.36	1.72	1.74
	H_a (Å)	−0.38	−0.28	−0.21	−0.28	0.48	1.91
	$d_{\mathrm{adatom-Ag}}$ (Å)	2.68	2.84	2.84	2.76	3.07	3.32
	d_{ST} (Å)	4.59	4.89	4.90	4.76	5.24	4.53
LT	E_a (eV)	3.08	2.91	2.16	2.31	1.65	1.82
	H_a (Å)	−0.40	−0.25	−0.09	0.34	1.35	2.03
	$d_{\mathrm{adatom-Ag}}$ (Å)	2.59	4.75	2.73	2.59	2.93	3.31
	d_{LT} (Å)	4.44	4.75	4.73	4.40	4.30	4.24
SiT	E_a (eV)	2.22	1.54	1.17	1.86	1.44	1.80
	H_a (Å)	−0.19	1.34	1.43	1.23	1.79	2.25
	$d_{\mathrm{adatom-Si}}$ (Å)	2.27	2.68	2.75	2.57	3.03	3.43
	d_{SiT} (Å)	3.70	2.55	2.55	2.59	2.57	2.56

For a clean $\sqrt{3}$-Ag or $\sqrt{21}$-Ag surface, the average Ag–Ag distance in the Ag layer is 3.45 Å [(3.85 + 3.06)/2 Å], which is larger than the Ag–Ag distance of bulk Ag (2.94 Å). Thus, the clean surface has much space to accommodate adatoms immersing into the Ag layer. Our results show that Cu, Au, Ag and Li adatoms can immerse into the substrate Ag layer due to their smaller atomic radii. The minus values of the adsorption heights in table 1 represent the depth of the adatoms incorporated into the Ag layer. It is easily to understand that the adatom Cu, having the smallest atomic radius, has the largest depth under the Ag layer. Adsorption of the adatoms induces the reconstruction of the Ag layer drastically. In table 1 the side lengths of the Ag triangles and Si trimers where the adatoms adsorb are given. Comparing the clean $\sqrt{21}$-Ag surface ($\sqrt{3}$-Ag phase), the side lengths of the Ag triangles and Si trimers are increased. As an example of the reconstruction, adsorption of a Na adatom at the ST site induces the substrate Ag layer with significant structural change: the area of the ST is expanded by 194% with an equilateral side length of 5.24 Å. The three neighboring LTs around the ST are shrunk by 37%, with side lengths of 2.85–4.00 Å. The adsorption energy at the ST site is larger, with a value of 1.72 eV. When the Na adatom adsorbs at the LT site, the area of the LT is expanded only by 10% and a 4% contraction of the three STs around the LT is observed. However, if the Na adatom is put on the SiT site, the side lengths of the LTs and the STs around the SiT site are almost unchanged, and the corresponding adsorption energy is smaller (1.44 eV).

It is interesting to compare our results with the adsorption coverage of ∼0.05 ($a\sqrt{21}$-Ag surface unit cell used) to that of Jeong *et al* [26] with a coverage of ∼0.02 ($a4\sqrt{3} \times 4\sqrt{3}$-Ag surface unit cell used). For the adsorption of noble adatoms, the adsorption energies at the LT and ST sites at the two coverages are almost the same, indicating weak interactions between the noble adatoms at low coverages due to their *d* electron screening. For the adsorption of alkali adatoms, however, the adsorption energies at the lower coverage ∼0.02

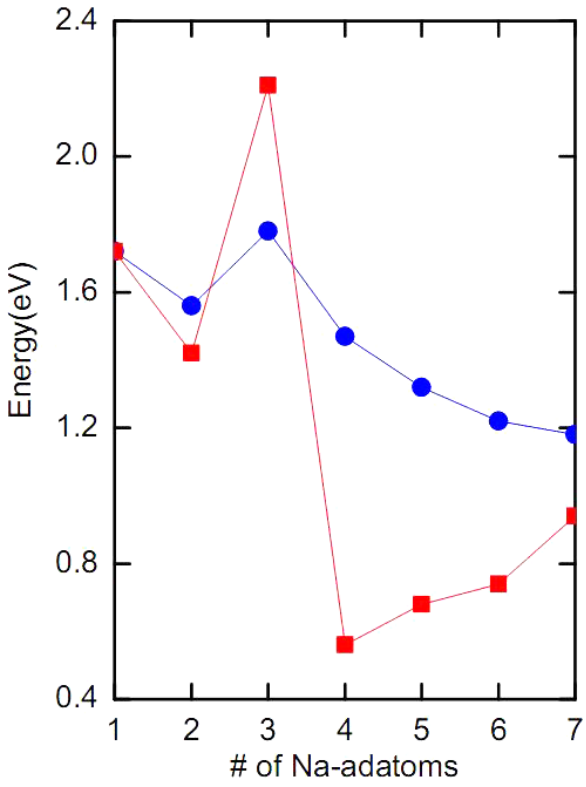

Figure 3. Calculated average adsorption energy (filled circles) and addition energy (filled boxes) in eV of Na adatom as a function of numbers of Na per unit cell. We only show the results for the most stable configurations of Na adsorptions for different coverages.

are more than those at the higher coverage ∼0.05 by at least 0.3 eV. Obviously, stronger repelling interactions exist between the adsorbed alkali adatoms due to the lack of electron screening.

Using the $\sqrt{21}$-Ag surface unit cell, we further study the coverage dependence of the adsorption properties and stability of the superstructure of $\sqrt{21}$-Ag+ adatoms. As pointed out in section 1, recently Jeong *et al* proposed, according to their first-principles calculations, that for Ag adatom adsorption a three-Ag adatom immersed structure on the $\sqrt{21}$-Ag surface was found to be the most favorable [21]. Here we further check the cases of alkali metal adsorption. We take Na as an example and add a Na adatom on the $\sqrt{21}$-Ag unit cell from one (1/21 ML) to seven adatoms (7/21 ML). In the $\sqrt{21}$-Ag unit cell each adsorption site (LT, ST or SiT) has seven equivalent adsorption positions. We put Na adatoms on these positions by finding all possible adsorption cases and relaxing them into the convergence structures. Finally, after testing several tens of adsorption configurations we find the most stable adsorption configurations for adsorption of one to seven Na adatoms in the unit cell. The most stable configurations at different coverages are shown schematically in figure 1 (labeled by numbers). The average and addition adsorption energies at different coverages are given in figure 3. The average adsorption energies at both LT and ST sites and addition energies for stable configurations are present in table 2.

For one Na adatom per unit cell, the adsorption energy is calculated to be 1.72 eV at the ST site, which has already

Table 2. Calculated average adsorption energies (E_a (eV)) for Na adatoms at LT and ST sites at different coverages. ST (LT) (1–7) represent adsorption of one to seven Na adatoms at the ST (LT) sites. The adsorption configurations are shown schematically in figure 1. Addition energy of the Na adatom (E_{add} (eV)) is defined as the absolute value of the total energy difference between a stable adsorption configuration with an extra adatom and a stable adsorption configuration plus an isolated adatom.

Sites	E_a	E_{add}
ST(1)	1.72	
LT(1)	1.65	
ST(12)	1.56	1.42
LT(12)	1.56	
ST(123)	1.60	
LT(123)	1.78	2.21
ST(1–4)	1.47	0.56
LT(1–4)	1.40	
ST(1–5)	1.32	0.68
LT(1–5)	1.26	
ST(1–6)	1.19	
LT(1–6)	1.22	0.75
ST(1–7)	1.17	
LT(1–7)	1.18	0.96

been mentioned above. For two Na adatoms, the calculated average adsorption energy is 1.56 eV per Na at two ST or LT sites, which is smaller than that of adsorption of one Na adatom, indicating repelling interactions between Na adatoms. For adsorption of three Na adatoms, however, the maximum average adsorption energy of 1.78 eV per Na is achieved as the three Na adatoms adsorb at the three LT sites which surround a ST site (see figure 4(a)) and the average adsorption height is 0.86 Å from the substrate Ag layer. For other adsorption configurations, for example, the three Na adatoms adsorb at the three ST sites (hereafter 3ST) around a LT site, where the average adsorption energy is 0.18 eV less per Na than for the most stable configuration; if the three Na adatoms are put on the three ST sites which surround a SiT, the superstructure becomes less stable by 0.04 eV than the most stable configuration. If we put the adatoms at the three LT sites which surround a SiT site, the average adsorption energy is almost the same as the adatoms at the three ST sites which surround a LT site.

We should note that the most stable configuration with three-Na adatom adsorption is different from that of the three-Ag adatom adsorption (see figure 4(b)), where the three Ag adatoms adsorb and immerse at the three ST sites which surround a LT site [21, 26]. However, interestingly, similar to the case of Ag adsorption, we find that the average adsorption energy of Na also drops as the coverage goes beyond 0.14 ML (three Na adatoms per $\sqrt{21}$-Ag unit cell), and then the average adsorption energy gradually decreases as the coverage increases. For the addition energy, which is defined as the adsorption energy to add an extra adatom on the surface, after experiencing a sharp decline at the coverage of 4/21 ML, it increases slightly as the coverage increases. Jeong *et al* [21] gave an explanation about the stabilization at the critical coverage of 0.14 ML of Ag adsorption. They argued that at the critical coverage the available space for adatom immersion is fully saturated, and the average distance between Ag

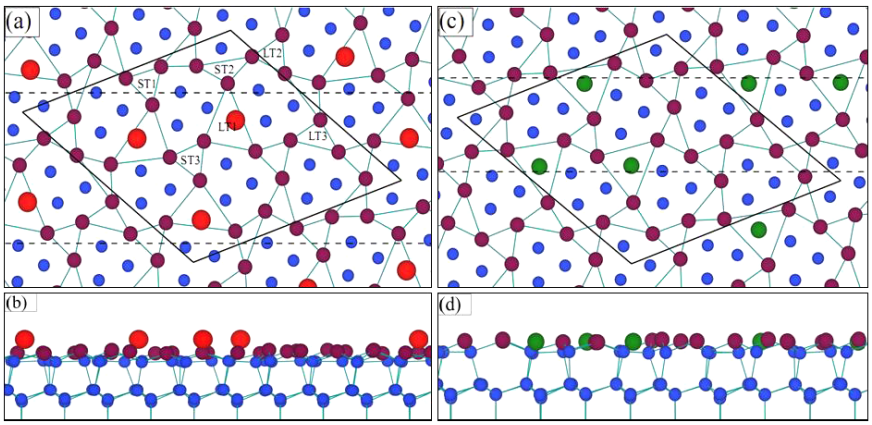

Figure 4. (a), (c) Top and (b), (d) side views of the most stable configurations of $\sqrt{21}$-Ag with three Na and Ag adatoms, respectively. Six characteristic Ag triangles, which are drastically changed from the large (LT1–LT3) and small (ST1–ST3) Ag triangles after adsorption of three Na adatoms, are shown in (a). The red and green atoms represent three Na and Ag adatoms, respectively.

atoms is drastically reduced so that the Ag–Ag bond strength is optimized at the coverage and the surface is therefore stabilized. This explanation seems reasonable and perfect. But one question still exists: why is the average adsorption energy of the two-Ag adatom immersed configuration smaller than that of one-Ag adatom immersed one? The Ag–Ag bond strength in the case with two immersed adatoms per unit cell should be more optimized than that of the case with one immersed adatom. According to Jeong's argument, the average adsorption energy of the former should be larger than the latter. However, this conclusion is in conflict with the calculated values. Thus, the optimized Ag–Ag bond strength should be only one of the reasons for the existence of the critical coverage 0.14 ML. In fact according to our following results for the electronic structures, we can find that the splitting and full filling of one of the surface states is another reason to stabilize the surface at the critical coverage. Adsorbed Na adatoms, on the other hand, do not incorporate into the substrate Ag layer due to their larger atomic radius. But the adsorption of Na adatoms on the surface still induces the drastic changes in the substrate Ag layer and reduces the average Ag–Ag distance. In the most stable configuration, Ag triangles with side lengths of 3.06 and 3.85 Å now turn into six characteristic triangles after adsorption of three Na adatoms (LT1–LT3 and ST1–ST3 shown in figure 4(a)). The area of the three large triangles (LT1) containing three Na adatoms is expanded by ∼51% (6.39 versus 9.63 Å^2 before and after the adsorption) with side lengths of 4.15–5.58 Å. The large Ag triangles (LT2 and LT3) are contracted by 43% and 38% with side lengths of 2.91 Å and 2.82–3.95 Å. The expansion of the LT1 also leads to the contraction of its neighboring small triangles (ST1–ST3). The area of the central small triangle (ST3) surrounded by the three Na adatoms (LT1) is shrunk by ∼6% (4.05 versus 3.82 Å^2) with equilateral side lengths of 2.97 Å. The contractions of the other two neighboring small triangles, ST1 and ST2, amount to 8% (3.73 Å^2) and 6% (3.79 Å^2) with side lengths of 2.91–2.96 Å and 2.80–4.50 Å, respectively. The seven Si trimers with original equilateral side lengths of 2.52 Å in a unit cell are classified into three kinds of triangles after adsorption. There is one Si triangle with an equilateral side of 2.56 Å, and there are two Si triangles with side lengths of 2.41–3.02 and 2.46–2.72 Å. Therefore, the Si trimers do not undergo large structural changes upon Na adsorption.

Table 3. Average adsorption energy in eV and adsorption height in Å of adsorption of three noble and alkali adatoms for various configurations. ST(123), LT(123), ST(234) and LT(234) represent the four different adsorption configurations corresponding to three-adatom adsorption at the three neighboring ST sites around a LT site, the three neighboring LT sites around a ST site, the three neighboring ST or LT sites around a SiT site, respectively.

Configuration		Cu	Au	Ag	Li	Na	K
ST(123)	E_a	3.26	3.27	2.43	2.34	1.60	1.64
	H_a	−0.34	−0.25	−0.15	−0.04	0.86	1.63
LT(123)	E_a	3.29	3.22	2.43	2.45	1.78	1.83
	H_a	−0.35	−0.25	−0.16	−0.04	0.86	1.58
ST(234)	E_a	3.38	3.17	2.40	2.43	1.74	1.80
	H_a	−0.29	−0.08	−0.02	0.11	0.88	1.61
LT(234)	E_a	3.21	3.30	2.43	2.30	1.61	1.67
	H_a	−0.22	−0.07	0.00	0.13	0.96	1.67

From experimental results, we know that monovalent adatoms on the $\sqrt{3}$-Ag surface may bring similar atomic and electronic structures. Similar to Ag adsorption, our results demonstrate that the configuration with three Na adatoms at the LT sites is the most stable phase. We therefore further investigate adsorption configurations of three other noble or alkali adatoms. The calculated average adsorption energy per adatom at different adsorption configurations and the corresponding adsorption heights are listed in table 3. On the one hand, three immersed Ag adatoms with an adsorption energy of 2.43 eV/Ag have four kinds of stable adsorption configurations which are 3ST surrounding a LT, 3LT surrounding a ST and 3ST or 3LT surrounding a SiT, respectively. The average adsorption energy at the four different adsorption sites is almost the same, which is in agreement with the results of Jeong *et al* [21]. The favorable adsorption configurations for three immersed Au and Cu adatoms are 3LT around a SiT and 3ST around a SiT, respectively. On the other hand, the most stable adsorption

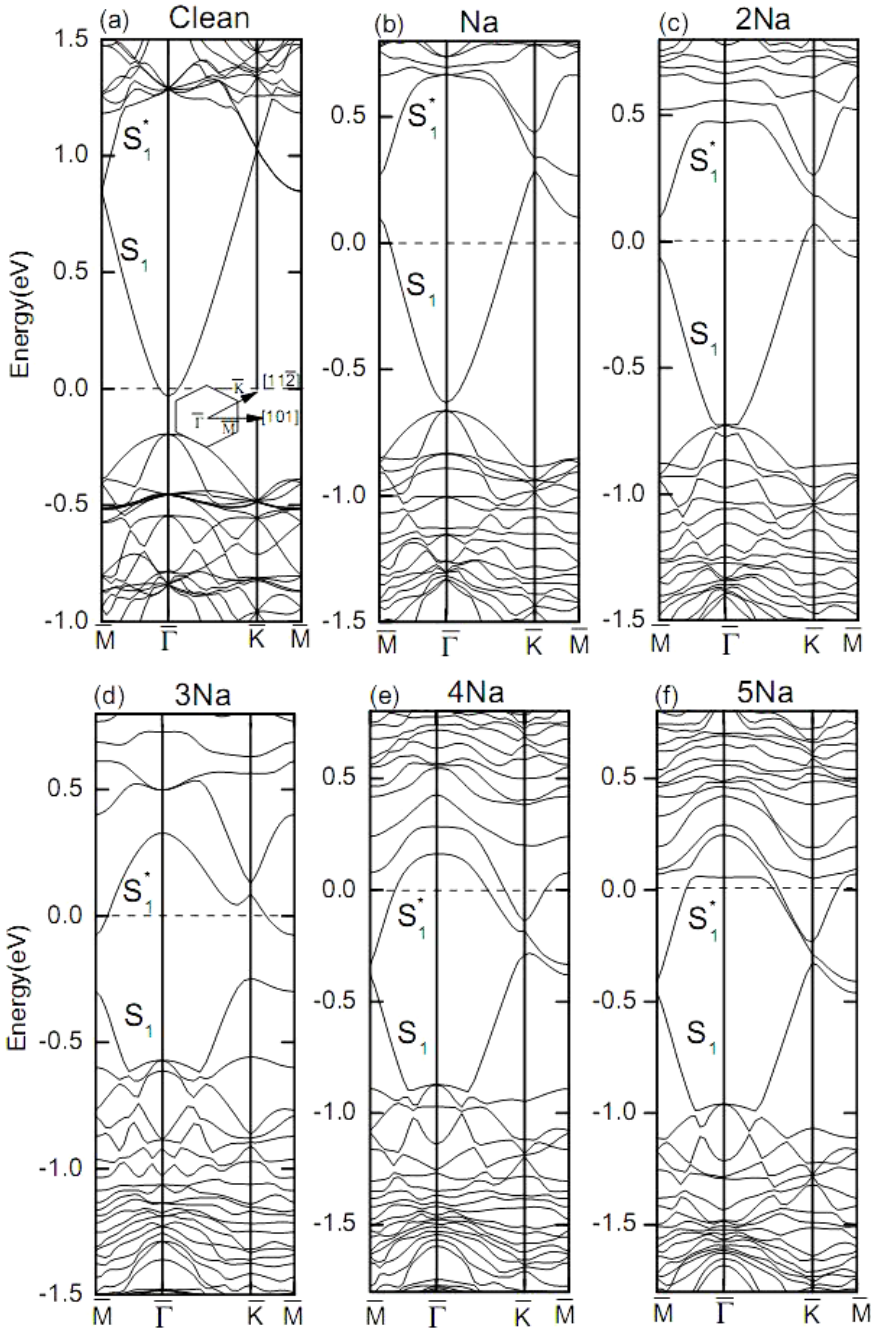

Figure 5. Calculated band structures for (a) clean $\sqrt{21}$-Ag, (b) $\sqrt{21}$-Ag+Na, (c) $\sqrt{21}$-Ag+2Na, (d) $\sqrt{21}$-Ag+3Na, (e) $\sqrt{21}$-Ag+4Na and (f) $\sqrt{21}$-Ag+5Na. The inset in (a) shows the SBZ of the $\sqrt{21}$-Ag surface unit cell. The energy zero is the Fermi level (E_F).

configurations are 3LT around a ST for all alkali adatoms. In general, the differences of the average adsorption energy for the four adsorption configurations are small (<0.2 eV) and the adsorption heights are almost the same. Adsorption of both noble and alkali adatoms at the critical coverage can induce significant structural changes of the substrate Ag layer and enhance the Ag–Ag bond strength.

3.2. Electronic structures

In order to further understand the features of the alkali metal adsorption on the $\sqrt{3}$-Ag surface, we calculate electronic structures of Na adsorption at different coverages as an example. The calculated band structures for the clean $\sqrt{21}$-Ag ($\sqrt{3}$-Ag phase) and Na adsorption surfaces with from one (0.05 ML) to five (0.24 ML) Na adatoms are presented in figure 5. For the clean $\sqrt{21}$-Ag surface, the parabolic dispersive surface band s_1 is clearly seen in the band gap of the bulk Si and exhibits an isotropic dispersion along different directions in figure 5(a), which is completely in agreement with a previous experimental observation [9]. The surface band s_1^* above the s_1 band is ascribed to band folding of the s_1 band of the $\sqrt{3}$-Ag surface unit cell and the s_1 band mainly

originates from the surface parallel components of Ag 5p contributions [15, 21, 33]. The Ag atoms saturate dangling bonds of the topmost Si atom and the clean surface has no dangling bonds. Therefore, the clean surface is a special case: it does not provide electrons for bonding, but provides an empty surface state s_1. Therefore, bonding possibly occurs between adatoms and the surface via filling electrons from adatoms into the surface state, which is different from the usual bonding on the surface where substrate atoms and adatoms provide electrons simultaneously to form covalent bonds by sharing electrons. For the band structure of the clean $\sqrt{21}$-Ag surface, the bottom of the s_1 band is somewhat below the Fermi level at Γ. Thus, the clean surface exhibits a weak metallic character at low temperature [4].

After doping one Na adatom on the surface (0.05 ML), an interesting change in the surface band s_1 can be seen in figure 5(b): it splits into two bands, s_1 and s_1^*, and a gap of about 0.2 eV is opened between the two bands at the SBZ boundary. Compared to the band structure of the clean surface, the two bands shift downward to higher binding energies and the s_1 band is partially filled, which again agrees with the experiment [9]. The band splitting with a gap opening is obviously due to the appearance of the ionic potential generated by the Na adatom on the surface: the Na adatom donates its 3s electron to the s_1 band, and the delocalized electron with a free-electron-like character feels the potential of the Na cation and in the periodic Na cation potential the s_1 band splits into a bonding surface state (s_1) and an anti-bonding surface state (s_1^*) with a gap between them. Two recent experiments by Crain *et al* [34] and Liu *et al* [35] pointed out that the s_1 band splits with a gap opening with a small number of adatoms at low temperatures, thanks to the hybridization of the s_1 band with an impurity state formed by the adatoms. However, they indicated that the splitting band is below the Fermi level. The DFT calculations of Jeong *et al* [21] for Ag adsorption gave a similar band structure with a small band splitting, but they ignored the splitting and the changes of the s_1 band and argued that the adsorption of extra Ag adatoms just induces a shift of the s_1 band. Our calculated band structures clearly demonstrate that the surface band s_1 splits into a bonding and an anti-bonding surface state and the two bands, along with other surface bands (not labeled in the figure), shift downwards to higher binding energies. At a coverage of 0.05 ML, the bonding state s_1 is partially occupied and the anti-bonding state is empty. The conductance of the surface should be enhanced.

For two-Na adatom adsorption (0.10 ML), the s_1 band continues to fill, but is still not full (see figure 5(c)). The two bands s_1 and s_1^* move downwards and at the bottom of the s_1 band, at Γ, the dispersion deviates from a parabolic character due to interaction with the other surface states. For three-Na adatom adsorption, which corresponds to the most stable surface phase with the critical coverage 0.14 ML, the band structure exhibits special features: the s_1 band is fully filled and the gap between s_1 and s_1^* is ∼0.25 eV, which is the largest gap for all coverages. At this coverage, few electrons are also occupying the anti-bonding state s_1^*. The large band gap between the bonding and anti-bonding states implies the stability of the system, which is in line with the calculated the largest average adsorption energy of the system.

As the coverage increase to 0.2 and 0.24 ML (four and five adatoms in the unit cell), from the band structures shown in figures 5(e) and (f) we can see that the anti-bonding state s_1^* is partially filled and the band gap between s_1 and s_1^* at the SBZ boundary is reduced. The Fermi level shifts upward to the conduction bands and the surface becomes metallic in nature.

4. Conclusion

Using density-functional theory within the generalized gradient approximation we investigated atomic and electronic structures of noble and alkali metal adatom adsorption on the $\sqrt{3}$-Ag surface. Our results show that the adsorption behaviors of the metal adatoms are closely related to their atomic size. A single adatom such as Ag Au, Cu or Li with a small atomic radius can immerse into the substrate Ag layer, while Na or K, with large atomic radii, adsorb on the surface. Adsorption of both noble and alkali adatoms, irrespective of incorporation into or on the surface, may induce significant changes in the atomic structure of the substrate Ag layer and reduce the average Ag–Ag distance. The most stable configurations of the adsorption systems are three noble or alkali adatoms in the unit cell. The three adatoms may incorporate into the LT or ST sites dependent on their atomic radii. For the electronic properties, we find that the almost empty two-dimensional free-electron-like band s_1 and its band folding s_1^* of the original surface band s_1 of $\sqrt{3}$-Ag split into two bands with a gap opening at the SBZ boundary with adatom adsorption. The two surface bands gradually move downwards and the bonding surface state s_1 gradually fills with increasing coverage. The s_1 band is fully occupied with the largest band gap of ∼0.25 eV between the s_1 and s_1^* bands at the critical coverage 0.14 ML (three adatoms in the $\sqrt{21}$-Ag unit cell), which corresponds to the most stable adsorption phase. Although the adsorption configurations are different, both noble and alkali adatom adsorption give rise to similar electronic structures at low coverages, indicating a free-electron-like character of the adsorption surfaces.

Acknowledgments

This work was supported by the National Science Foundation of China (grant nos 10974182, 10874154), and we are grateful to Dr Hojin Jeong for beneficial discussions.

References

[1] Uhrberg R I G and Hansson G V 1991 *Crit. Rev. Solid State Mater. Sci.* **17** 133
[2] Lee K D and Chung J 1998 *Phys. Rev.* B **57** R2053
[3] Matsuda I, Yeom H W, Tono K and Ohta T 1999 *Phys. Rev.* B **59** 15784
[4] Hasegawa S, Tong X, Takeda S, Sato N and Nagao T 1999 *Prog. Surf. Sci.* **60** 89
[5] Matsuda I, Morikawa H, Liu C, Ohuchi S, Hasegawa S, Okuda T, Kinoshita T, Ottaviani C, Cricenti A, Dangelo M, Soukiassian P and LeLay G 2003 *Phys. Rev.* B **68** 085407

[6] Hasegawa S, Sato N, Shiraki I, Petersen C L, Boggild P, Hansen T M, Nagao T and Grey F 2000 *Japan. J. Appl. Phys.* 1 **39** 3815
[7] Takahashi T, Tajiri H and Sumitani K 2003 *Surf. Rev. Lett.* **10** 519
[8] Nogami J 1994 *Surf. Rev. Lett.* **1** 395
[9] Matsuda I, Hirahara T, Konishi M, Liu C, Morikawa H, D'angelo M, Hasegawa S, Okuda T and Kinoshita T 2005 *Phys. Rev.* B **71** 235315
[10] Nakajima Y, Takeda S, Nagao T, Hasegawa S and Tong X 1997 *Phys. Rev.* B **56** 6782
[11] Tong X, Jiang C S and Hasegawa S 1998 *Phys. Rev.* B **57** 9015
[12] Tajiri H, Sumitani K, Yashiro W, Nakatani S, Takahashi T, Akimoto K, Sugiyama H, Zhang X and Kawata H 2001 *Surf. Sci.* **493** 214
[13] Zhang H M, Sakamoto K and Uhrberg R I G 2001 *Phys. Rev.* B **64** 245421
[14] Crain J N, Altmann K N, Bromberger C and Himpsel F J 2002 *Phys. Rev.* B **66** 205302
[15] Tong X, Ohuchi S, Sato N, Tanikawa T, Nagao T, Matsuda I, Aoyagi Y and Hasegawa S 2001 *Phys. Rev.* B **64** 205316
[16] Hasegawa S 2000 *J. Phys.: Condens. Matter* **12** R463
[17] Tong X, Jiang C S, Horikoshi K and Hasegawa S 2000 *Surf. Sci.* **449** 125
[18] Ichimiya A, Nomura H and Horio Y 1994 *Surf. Rev. Lett.* **1** 1
[19] Nogami J, Wan K J and Lin X F 1994 *Surf. Sci.* **306** 81
[20] Tong X, Ohuchi S, Tanikawa T, Harasawa A, Okuda T, Aoyagi Y, Kinoshita T and Hasegawa S 2002 *Appl. Surf. Sci.* **190** 121
[21] Jeong H, Yeom H W and Jeong S 2008 *Phys. Rev.* B **77** 235425
[22] Liu C, Matsuda I, Morikawa H, Okino H, Okuda T, Kinoshita T and Hasegawa S 2003 *Japan. J. Appl. Phys.* 1 **42** 4659
[23] D'angelo M, Konishi M, Matsuda I, Liu C, Hasegawa S, Okuda T and Kinoshita T 2005 *Surf. Sci.* **590** 162
[24] Konishi M, Matsuda I, Liu C, Morikawa H and Hasegawa S 2005 *Surf. Sci. Nanotechnol.* **3** 107
[25] Hasegawa S, Tsuchie K, Toriyama K, Tong X and Nagao T 2000 *Appl. Surf. Sci.* **162/163** 42
[26] Jeong H, Yeom H W and Jeong S 2007 *Phys. Rev.* B **76** 085423
[27] Kresse G and Hafner J 1993 *Phys. Rev.* B **47** R558
Kresse G and Furthmüller J 1996 *Phys. Rev.* B **54** 11169
[28] Vanderbilt D 1990 *Phys. Rev.* B **41** 7892
[29] Perdew J P and Wang Y 1992 *Phys. Rev.* B **45** 13244
[30] Sasaki N, Watanabe S and Tsukada M 2002 *Phys. Rev. Lett.* **88** 046106
[31] Aizawa H, Tsukada M, Sato N and Hasegawa S 1999 *Surf. Sci.* **429** L509
[32] Tajiri H, Sumitani K, Nakatani S, Nojima A, Takahashi T, Akimoto K, Sugiyama H, Zhang X and Kawata H 2003 *Phys. Rev.* B **68** 035330
[33] Aizawa H and Tsukada M 1999 *Phys. Rev.* B **59** 10923
[34] Crain J N, Gallagher M C, McChesney J L, Bissen M and Himpsel F J 2005 *Phys. Rev.* B **72** 045312
[35] Liu C, Matsuda I, Hobara R and Hasegawa S 2006 *Phys. Rev. Lett.* **96** 036803